

Lifting, welding, and packaging of a quality-factor-controllable micromachined inductor using magnetic fields

Yu-Che Huang

National Tsing Hua University
Department of Power Mechanical Engineering
No. 101, Section 2, Guang-fu Road
Hsinchu 30013 Taiwan

Ben-Hwa Jang

Industrial Technology Research Institute
Material and Chemical Research Laboratory
Room 607, Building 52, 195, Section 4
Chung Hsing Road
Chutung, Hsinchu 310 Taiwan

Weileun Fang

National Tsing Hua University
Department of Power Mechanical Engineering
and
Institute of NanoEngineering and MicroSystems
Hsinchu 30013 Taiwan
E-mail: fang@pme.nthu.edu.tw

Abstract. This study demonstrates a novel approach to lift the inductor from the lossy substrate by static magnetic field. The lift angle of the inductor, which tuned by a position stage, is employed to control the quality factor of the inductor. The lifted inductor is then welded by localized induction heating using the ac magnetic field. Thus, the heating-induced thermal problem is prevented. In addition, the inductor is also simultaneously packaged inside a Si capping by the alternating magnetic field. To demonstrate the feasibility of the proposed concept, the meander strip inductor was fabricated and tested. The radio frequency performance of the inductor at various tilting angles away from the substrate (0, 45, and 90 deg) was characterized by using a two-port vector network analyzer. The quality factor has been improved from 4.2 (at the central frequency of 0.64 GHz) to 7.9 (at the central frequency of 0.74 GHz), as the lift angle increased from 0 to 90 deg. In other words, the central frequency of the inductor can also be varied from 0.64 to 0.74 GHz. Measurement results also indicate that the bonded Si capping has a good shear strength of 23.5 MPa. © 2010 Society of Photo-Optical Instrumentation Engineers. [DOI: 10.1117/1.3528431]

Subject terms: RF-MEMS inductor; localize welding; self-assembly.

Paper 10107R received Sep. 10, 2010; revised manuscript received Oct. 27, 2010; accepted for publication Nov. 3, 2010; published online Dec. 27, 2010.

1 Introduction

The rapid development of wireless communication systems requires the use of high-performance radio frequency (RF) inductors in the design of both monolithic microwave integrated circuits and RF integrated circuits. Thus, the high-performance inductors are the key components for implementing critical building blocks such as low phase-noise voltage-controlled oscillators (VCOs), low-loss impedance matching networks, passive filters, and power amplifiers. Critical parameters of the inductor include inductance value (L), quality factor, self-resonant frequency (f_{res}), and the area of the inductor. In order to evaluate the performance of the inductor, the unique figure of merit of an inductor [(FMI), i.e., $\text{FMI} = Q * f_{\text{res}} / \text{inductor area}$] is proposed.^{1,2} The high-performance inductor is with the large value of FMI. To obtain a larger FMI, the inductor with a high-quality factor, a high self-resonance frequency, and a small area are desirable.

Because of undesirable energy dissipation through substrate, the conventional planar on-chip inductors are with low-quality factor. To enlarge the value of FMI, many reducing substrate loss methods, such as solder surface tension self-assembly,³ the inductor suspended over a deep cavity by using bulk etch,⁴ on-chip suspended-spiral inductor,⁵ and plastic deformation magnetic assembly,⁶ which, based on the microelectromechanical system (MEMS) technology, have been reported to create physical separation between the inductor coil and the lossy substrate. Furthermore, tunable inductors can achieve the performance optimization of intelligent RF front-end circuits, such as adjusting the

central frequency of a bandpass filter, changing impedance of a matching network, and tuning the oscillation frequency of VCOs.⁷ The 3-D variable spiral inductor has been reported by using metallic glass.⁸ The variable inductor embedded in a Si CMOS chip is achieved by moving a metal plate above the inductor.⁹ However, the integration of the inductor and the positioning apparatus of metal-plate shielding is a critical concern.

In spite of the various improvements of the inductor's quality factor brought by the aforementioned methods, how to encapsulate the fragile MEMS inductor for protection and stabilizing of RF characteristics is also a critical issue. Because of inherent self-alignment during the solder reflowing, the solder bonding technique is one of the popular methods for wafer-level packaging of MEMS devices; however, the device needs to be heated up to 183°C to melt the solder for packaging. This temperature can also damage the MEMS structures with thin-film materials. The local heating method for wafer-level packaging of MEMS devices is reported in Ref. 10. The magnetic film (Ni) was electroplated under the solder. By applying time-varying external magnetic field, the magnetic film will be heated up due to the induction heating and leads to reflow the solder. The experiment results show that the temperature distribution in the MEMS devices region is much lower than the one in the soldering region. Thus, the MEMS structures would not be damaged during the reflowing process. In this study, we presented a quality-factor-controllable and self-assembly inductor integrated with a local heating method for packaging. Consequently, the RF performance of the inductor can be enhanced and the packaging process is more cost effective.

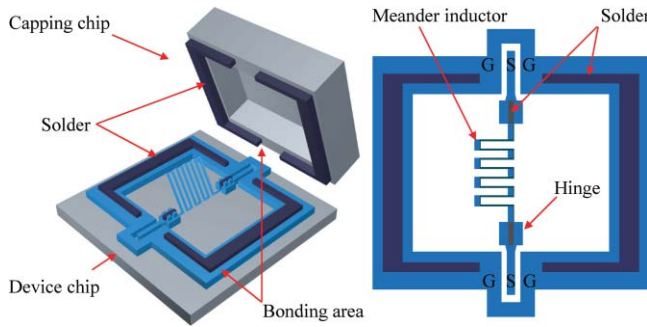


Fig. 1 Scheme of the proposed design: the bird's eye view of the device and the top view of the device chip.

2 Design and Concept

As discussed in Ref. 11, it is possible to increase the quality factor of the inductor by reducing the dissipation of energy from the substrate. In this regard, the approach to lift up the micromachined structures from substrate using the dc magnetic field¹² is employed in this study. Thus, the substrate loss will be varied by lifting the inductor from substrate, and the quality factor of inductor can be controlled. Figure 1 shows a schematic diagram of the proposed quality-factor-controllable micromachined inductor. It consists of two major components: the device chip and the capping chip. The device chip can be further decomposed into a meander inductor, two hinges, and two sets of ground-signal-ground pads for RF characterizing. The inductor is free to rotate around the hinges before the welding process. Moreover, the solder defines the welding area for the inductor as well as the bonding area for the capping chip. The magnetic field consists of both ac and a permanent magnet, which was applied to the device after the capping chip had been placed on the device chip. Thus, the inductor was lifted up from the substrate by magnetic field that provided by a permanent magnet; meanwhile, the inductor was welded on the substrate and two chips were bonded together by the ac magnetic field.

Figure 2 shows the details of the lifted and welded inductor, and the bonded capping chip. Figure 2(a) shows the top and side views of the substrate during the lifting of the inductor. The inductor is designed to consist of a Ni/Cu/Ni sandwich structure. The advantages of such a symmetrical sandwich structure are to prevent oxidization of the copper layer and to reduce thermal bending of the Ni/Cu/Ni structure. Because nickel is a ferromagnetic material, the Ni/Cu/Ni inductor is under a magnetic force after applying a magnetic field that was provided by a permanent magnet. As the side view of the substrate shows in Fig. 2(a), the inductor will rotate around the hinge until its equilibrium position is coincident with the magnetic field. In this study, the direction of magnetic field is fixed and thus the tilting angle of the lifted inductor θ with the silicon substrate can be precisely defined by an angular position stage. After that, an ac magnetic field is then applied on the substrate. As the top view of substrate indicates in Fig. 2(a), the hinges are surrounded with Ni and solder films. The eddy current will be induced in the Ni film after applying the ac magnetic field.¹⁰ The Ni film will act as the heater to heat and melt the solder. After removing the magnetic field, the temperature of Ni film is dropped and the solder will be solidified to weld the inductor. Finally, the

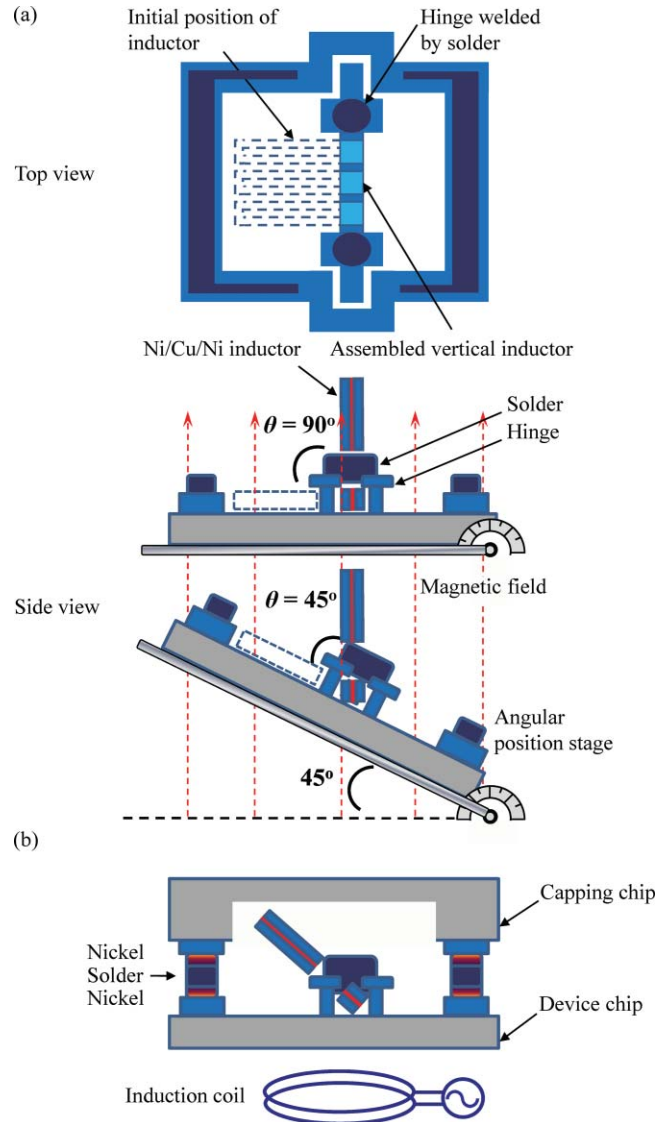


Fig. 2 The concept of this study: (a) the top and side views show the lifting and welding of the inductor by magnetic field, and (b) the bonding of inductor substrate and the capping wafer by ac magnetic field. The welding of the lifted inductor and the bonding of the capping wafer can be accomplished simultaneously by the ac magnetic field.

magnetic field can be removed. Thus, the welded inductor at the tilt angle θ is achieved. As the tilt angle θ of the inductor is increased, less magnetic flux lines are associated with the excitation current penetrate through the silicon substrate, resulting in a decrease of the inductive substrate loss, and then the quality factor can be changed. Similarly, the Ni film for localized heating is also electroplated under the solder for bonding the capping chip, as shown in Fig. 2(b). Thus, welding of the lifted inductor and bonding of the capping wafer are accomplished simultaneously by the ac magnetic field.

3 Fabrication and Results

This study also established the process of demonstrating the fabrication and packaging of the inductor. Figures 3(a) and 3(b) respectively illustrate the process steps to realize the proposed inductor and the capping wafer. As illustrated in

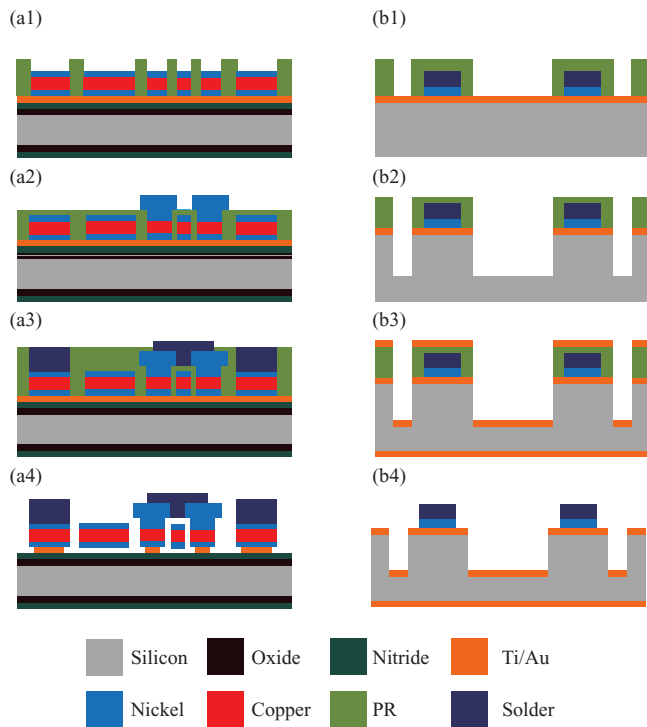


Fig. 3 Fabrication process steps for (a) the inductor and (b) the capping wafer.

Fig. 3(a), the processes began with the thermal growth of $1\ \mu\text{m}$ silicon dioxide on a silicon wafer, and then the deposition of $500\ \text{nm}$ of silicon nitride film by low-pressure chemical vapor deposition. The silicon nitride film was used as the protection layer for silicon oxide during the following Ti etching. After that, a 100-nm -thick titanium (Ti) film and a 200-nm -thick gold (Au) film were evaporated onto the silicon substrate as the adhesive and seed layers, respectively. As shown in Fig. 3(a1), after the photolithography of a thick photoresist, the electroplating of nickel/copper/nickel ($2.5\ \mu\text{m}/15\ \mu\text{m}/2.5\ \mu\text{m}$) was employed to form a $20\text{-}\mu\text{m}$ thick inductor. As shown in Fig. 3(a2), the photoresist was exploited to define the moving space for the hinge, and the electroplated Ni was employed to fabricate the hinge. As shown in Fig. 3(a3), the photolithography and electroplating processes defined the dimensions and location of the solder (Sn63/Pb37) on the Ni plate. As shown in Fig. 3(a4), after removing the photoresist and the Ti/Au layers, the Ni/Cu/Ni inductor was released from the substrate. The Ti and Au films were respectively removed using the buffer oxide etcher (BOE) and the etchant of $\text{KI}/\text{I}_2/\text{H}_2\text{O}$ ($\text{KI}:\text{I}_2:\text{H}_2\text{O} = 4:1:40$). Note that the anchor of hinge is undercut during the removal of Ti/Au. The planar dimensions of the inductors and hinges must be properly designed to shorten the releasing time of inductor and to reduce the undercut of the hinge anchor. Thus, the hinge can firmly anchor to the substrate after the full release of inductor. As shown in Fig. 3(b1), the capping wafer was evaporated with 20-nm Ti and 200-nm Au films as the adhesive and seed layers, respectively. The electroplating and lift-off processes were employed to pattern a $5\text{-}\mu\text{m}$ Ni and $15\text{-}\mu\text{m}$ solder as the bonding area. After a $20\text{-}\mu\text{m}$ -thick photoresist was patterned as the etching mask, deep reactive

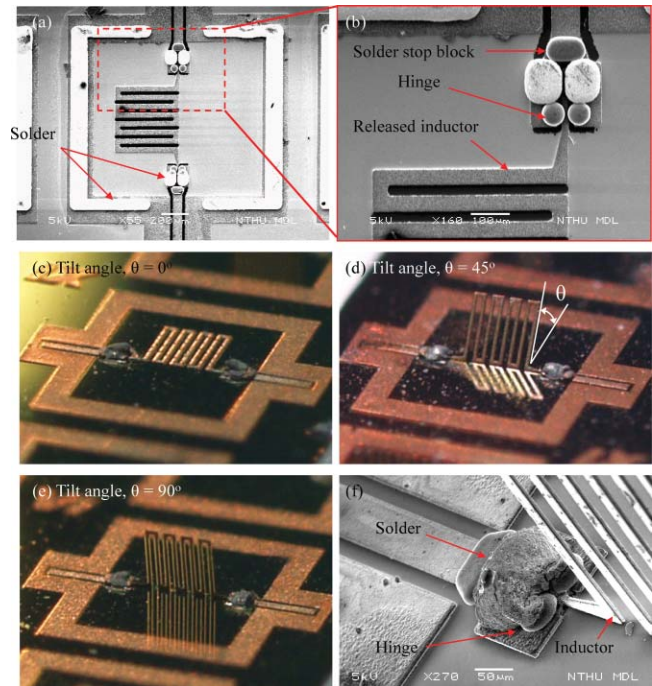


Fig. 4 Image of typical fabrication results: (a) the SEM image of the inductor before assembly, (b) zoom-in of the electroplated solder before welding, (c–e) the self-assembly inductors, respectively, at tilt angles of 0° , 45° , and 90° , and (f) the zoomed-in SEM image of the hinge welded by solder.

ion etching was employed to define the space to allow the inductor to be lifted vertically on the substrate, as shown in Fig. 3(b2). As shown in Figs. 3(b3) and 3(b4), the Ti/Au films were evaporated and patterned by the lift-off process on both the front and back sides of substrate for metallization. The metallized surfaces of the cavity served both as a good ground and as an electromagnetic shield to isolate the inductor from its environment.¹³ As a result, the inductor in Fig. 3(a4) was ready to be lifted and welded. Meanwhile, the substrate in Fig. 3(a4) was also ready to be bonded with the capping wafer in Fig. 3(b4).

To demonstrate the feasibility of the proposed inductor, this study applied a strong dc magnetic field by a SmCo permanent magnet to lift up the inductor from the substrate. The magnet is $12.7\ \text{mm}$ in diameter and $8\ \text{mm}$ thick, and has a maximum energy density $26.32\ \text{MGsOe}$. The magnet is placed above the device chip and is $2\ \text{cm}$ away from the center of the chip. Moreover, this study employed commercial equipment (KSP SP-30KW, Proking Heating Technologies International Corporation, Taichung, Taiwan) to apply ac magnetic field for induction heating. The operating frequency ranged from 78 to $87\ \text{kHz}$, and the magnetic flux density was $0.012\text{--}0.027\ \text{Tesla}$. During the welding and bonding process, the temperatures of electroplated solder achieved were in the range of $200\text{--}240^\circ\text{C}$, as measured by an infrared thermometer. Thus, the solder, which has a melting point of 183°C , melt for welding and bonding.

The scanning electron microscopy (SEM) image in Fig. 4(a) shows the fabricated inductor before assembly. The zoomed-in SEM image in Fig. 4(b) shows the electroplated solder before welding process. Figures 4(c)–4(f) show

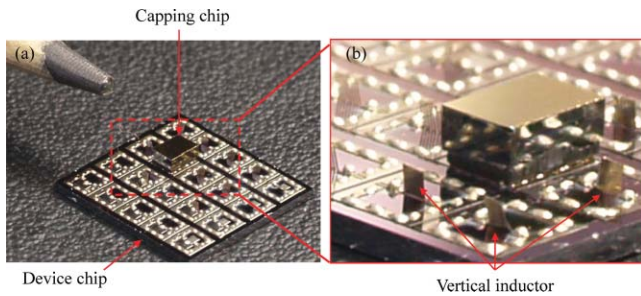


Fig. 5 Photos of typical bonding results: (a) one inductor chip bonded with a capping chip, (b) zoomed-in image of the capping chip, and the capping chip surrounded with the lifted and welded inductors is observed.

the fabricated inductors after assembled. As indicated in Figs. 4(c)–4(e), the inductors are respectively welded with tilt angles of 0, 45 and 90 deg. In addition, the zoomed-in SEM image in Fig. 4(f) shows the inductor hinge welded by solder after assembly. Figure 5(a) further shows the substrate with a lifted inductors array, and one of the lifted inductors is bonded with a capping chip. As demonstrated in Fig. 5(b), the capping chip is surrounded by inductors with a lifted angle of 90 deg. The solder bumps after reflow by the induction heating process are also observed.

4 Measurement and Discussion

The proposed inductor’s characteristics are measured by a vector network analyzer using a ground-signal-ground probe with a pitch of 100 μm. Figure 6 shows the scheme of the experimental setup. On-wafer measurements are typically calibrated using a ceramic impedance standard substrate that offers high accuracy and low loss standards for two-port calibration procedures, such as short-open-load-through calibrations. Two-port *S* parameters are measured and converted to *Y* parameters. As shown in Fig. 6(b), the open-pad structure can be used to de-embed the parasitic of the device under test. The *Y* parameters (Y_{ind}) of the inductor [intrinsic inductor shown in Fig. 6(c)] were obtained from measured *Y*

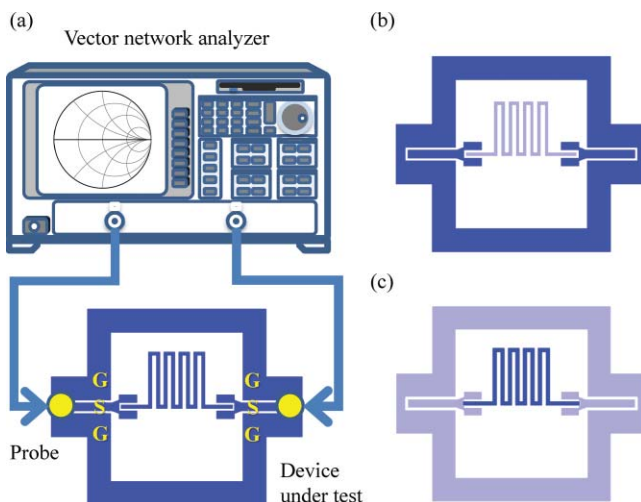


Fig. 6 Experimental setup.

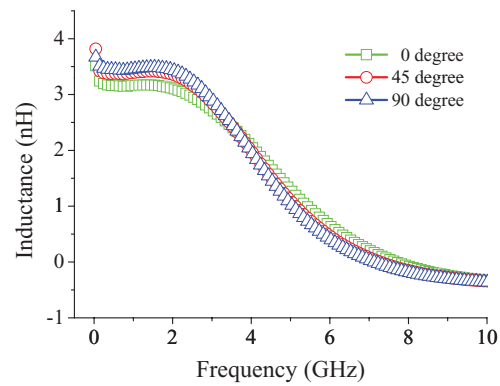


Fig. 7 Measured inductances at different tilt angles.

parameters (Y_{meas}) and *Y* parameters (Y_{pad}) of the open pad,

$$Y_{ind} = Y_{meas} - Y_{pad} \quad (1)$$

After de-embedding the parasitic of the probe pads, the quality factor and inductance can be obtained by calculating the following:

$$L = \frac{1}{\omega} \text{Im} \left(-\frac{1}{Y_{11}^{ind}} \right), \quad (2)$$

$$Q = \frac{\text{Im} \left(-\frac{1}{Y_{11}^{ind}} \right)}{\text{Re} \left(-\frac{1}{Y_{11}^{ind}} \right)}. \quad (3)$$

Figure 7 shows the measurement result of inductance as tilt angle θ between the inductor and the substrate, varying from 0 to 90 deg. Because of the skin effect, inductance decreases with increasing frequency. However, the θ has no significant influence on the inductance. Typical measurement results indicate the quality factor can be controlled within 4.2 (at the central frequency of 0.64 GHz) to 7.9 (at the central frequency of 0.74 GHz) by assembly, as shown in Fig. 8. In short, as the inductor tilt angle changes from 0 to 90 deg, the quality factor was improved by 88.5%. The quality factor was improved by 64.6% when the tilt angle moved from 0 to 45 deg. Moreover, the central frequency of the inductor can be varied from 0.64 to 0.74 GHz, as the lift angle increased from 0 to 90 deg.

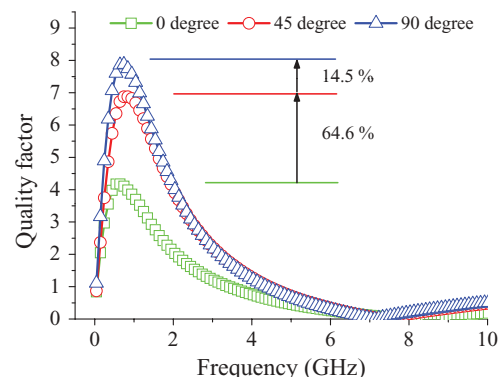


Fig. 8 Measured quality factors at different tilt angles.

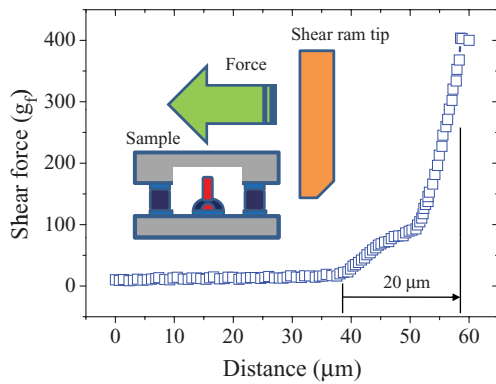


Fig. 9 Scheme of shear strength testing and the measurement results.

The shear strength of the bonded capping chip was measured by using a commercial shear tester. The bonding area was 0.23 mm^2 . The measurement result is shown in Fig. 9. The typical bonding strength is 403 g when the capping chip is with a displacement of $20 \mu\text{m}$ (from 38 to $58 \mu\text{m}$). The bonding shear strength measured for three different tests ranged from 17.2 to 23.5 MPa. After the shear test, the broken area of either the device or capping chips occurred at the silicon substrate instead of at the solder bonding region. Similar results have also been observed in Ref. 10. Referring to the shear strength measurement, solder bonding by the local heating technique can provide enough strength for the package application.

5 Conclusions

This study demonstrates a novel approach to lift the inductor from a lossy substrate by static magnetic field. Furthermore, the lifted inductor is then welded by localized induction heating using the ac magnetic field. Because the inductive loss depends on the tilt angle of the inductor, the quality factor and central frequency of the inductor can be easily tuned by varying the tilt angle. In addition, the inductor is also simultaneously packaged inside a Si capping by the alternating magnetic field. Because the local induction heating technique is employed for welding and bonding, the thermal problems induced by heating are prevented. In applications, the meander strip inductor was fabricated and tested. Experiment results indicate the quality factor of inductor has been improved from 4.2 to 7.9, as the lift angle increased from 0 to 90 deg. Moreover, the central frequency of inductor can also be varied from 0.64 to 0.74 GHz. Measurements also indicate that the bonded Si capping has good shear strength.

Acknowledgments

This project was supported, in part by the Ministry of Economic Affairs of Taiwan, under Contract No. 97-EC-17-A-08-S1-03. The authors also extend their appreciation to the Center of Nanotechnology, Materials Science, and Microsystems of National Tsing Hua University, the Nano Facility Center of National Chiao Tung University, and the National Nano Device Laboratory for providing the fabrication facilities.

References

1. I. J. Bahl, "High-performance inductors," *IEEE Trans. Microwave Theory Techniques*, **49**(4), 654–664, (April 2001).
2. I. J. Bahl, *Lumped Elements for RF and Microwave Circuits*, Artech House, Boston, (2003).
3. G. W. Dahlmann, E. M. Yeatman, P. R. Young, I. D. Robertson, and S. Lucyszyn, "MEMS high Q microwave inductors using solder surface tension self-assembly," in *Proc. of IEEE MTT-S Digest*, Phoenix, pp. 329–332 (May 2001).
4. H. Jiang, Y. Wang, J.-L. Andrew Yeh, and N. C. Tien, "On-chip spiral inductors suspended over deep copper-lined cavities," *IEEE Trans. Microwave Theory Techniques*, **48**(12), 2415–2423 (2000).
5. J.-B. Yoon, B.-K. Kim, C.-H. Han, E. Yoon, and C.-K. Kim, "CMOS-compatible surface-micromachined suspended-spiral inductors for multi-GHz silicon RF ICs," *IEEE Electron Dev. Lett.*, **20**, 487–489 (1999).
6. J. Chen, J. Zou, C. Liu, J. E. Schutt-Aine, and S.-M. Kang, "Design and modeling of a micromachined High-Q tunable capacitor with large tuning range and a vertical planar spiral inductor," *IEEE Trans. Electron Dev.*, **50**, 730–739 (2003).
7. I. Zine-EI-Abidine, M. Okoniewski, and J. G. McRory, "A new class of tunable RF MEMS inductors," in *Proc. of IEEE MEMS, NANO, and Smart Systems (ICMENS'03)*, Banff, Canada, pp. 114–115 (July 2003).
8. Y. Yokoyama, T. Fukushima, S. Hata, K. Masu, and A. Shimokohbe, "Fabrication and evaluation of an on-chip micro-variable inductor," *Jpn. J. Appl. Phys.*, **42**, 2190–2192 (2003).
9. H. Sugawara, Y. Yokoyama, S. Gomi, H. Ito, K. Okada, H. Hoshino, H. Onodera, and K. Masu, "Variable RF inductor on Si CMOS chip," *Jpn. J. Appl. Phys.*, **43**, 2293–2296 (2004).
10. H.-A. Yang, M. Wu, and W. Fang, "Localized induction heating solder bonding for wafer level MEMS packaging," *J. Micromech. Microeng.*, **15**, 394–399 (2005).
11. Y.-C. Huang, B.-H. Jang, and W. Fang, "Magnetic lifting and welding to simultaneously assembly and package a quality-factor-controllable micromachined inductor," presented at the *5th Asia-Pacific Conf. on Transducers and Micro-Nano Technology (APCOT2010)*, Perth, Australia (July 2010).
12. J. W. Judy, "Batch-fabricated ferromagnetic microactuators with silicon flexures," PhD dissertation, Dept. of Electrical Engineering and Computer Sciences, University of California, Berkeley (1996).
13. H. W. Ott, *Electromagnetic Compatibility Engineering*, Rev. ed., Wiley, Hoboken, NJ (2009).



Yu-Che Huang received his BS and MS at the Aerospace and System Engineering Department, Feng Chia University, Taiwan, in 2002 and 2004, respectively. He is currently working toward a PhD at the Power Mechanical Engineering Department, National Tsing Hua University, Taiwan. His major research interests include RF MEMS, LIGA-like fabrication process, and finite element analysis.



Ben-Hwa Jang received his BS in mechanical engineering from Tatung Institute of Technology (renamed Tatung University in 1999) in 1993; MS from the Institute of Biomedical Engineering, National Yang-Ming University, Taiwan, in 1995; and PhD from the Institute of NanoEngineering and MicroSystems, National Tsing Hua University, Taiwan, in 2009. Since 1997, he has been a researcher with the Material and Chemical Laboratories of Industrial Technology Research Institute in Taiwan. His current research interests include magnetic multiphysical design, analysis, modeling, and measurement for RF integrated passive devices and high-speed digital systems. He also has been a consultant to many enterprises for providing solutions on high-end connector design, high-speed PCB design, EMI, and related applications.



the NEMS Institute. In 1999 he was a visiting associate at California Institute of Technology. His research interests include MEMS with emphasis on microfabrication/-packaging technologies, CMOS MEMS,

Weileun Fang received his PhD from Carnegie Mellon University in 1995. His doctoral research focused on determining the mechanical properties of thin films using micromachined structures. In 1995, he worked as a postdoctoral researcher at the Synchrotron Radiation Research Center, Taiwan. He joined the Power Mechanical Engineering Department at National Tsing Hua University (Taiwan) in 1996, where he is now a professor as well as a faculty member at

CNT MEMS, micro-optical systems, micro-sensors and actuators, and characterization of thin-film mechanical properties. He is now a board member on *Journal of Micromechanics and Microengineering* and an associate editor of *Journal of Micro/Nanolithography, MEMS, and MOEMS*. He has served as the chief delegate of Taiwan for the World Micromachine Summit since 2008 and also as the TPC of IEEE MEMS'04, MEMS'07, and MEMS'10, the regional TPC of Transducers'07, and the EPC of Transducers'09. He became a member of the international steering committee of Transducers in 2009. He also serves as a technical consultant for many MEMS companies in Taiwan.